Configuration optimization of series flow double-effect water-lithium bromide absorption refrigeration systems by cost minimization

Sergio F. Mussati[a], Stefano Cignitti[b], Seyed Soheil Mansouri[b], Krist V. Gernaey[b], Tatiana Morosuk[c], Miguel C. Mussati[a],*

[a] *INGAR Instituto de Desarrollo y Diseño (CONICET − UTN), Avellaneda 3657, S3002GJC Santa Fe, Argentina*
[b] *Process and System Engineering Center (PROSYS), Department of Chemical and Biochemical Engineering, Technical University of Denmark, Søltofts Plads, Building 229, 2800 Kgs. Lyngby, Denmark*
[c] *Technische Universität Berlin, Institute for Energy Engineering, Marchstr. 18, 10587 Berlin, Germany*

ARTICLE INFO

ABSTRACT

An optimal process configuration for double-effect water-lithium bromide absorption refrigeration systems with series flow – where the solution is first passed through the high-temperature generator – is obtained by minimization of the total annual cost for a required cooling capacity. To this end, a nonlinear mathematical programming approach is used. Compared to the optimized conventional double-effect configuration, the new optimal configuration obtained in this paper allows reducing the total annual cost, the capital expenditures, and the operating expenditures by around 9.5%, 11.1% and 4.9%, respectively. Most importantly, the obtained optimal solution eliminates the low-temperature solution heat exchanger from the conventional configuration, rendering a new process configuration. The energy integration between the weak and strong lithium bromide solutions (cold and hot streams, respectively) takes place entirely at the high-temperature zone, and the sizes and operating conditions of the other process units change accordingly in order to meet the problem specification with the minimal total annual cost. This new configuration was obtained for wide ranges of the cooling capacity (150–450 kW) and the temperature of the cooling water (15–35 °C). The results of this work motivate to apply the simultaneous optimization approach to seek for new multi-effect absorption refrigeration system configurations with parallel and reverse flow as well as other series flow arrangements that minimize the total annual cost.

1. Introduction

Today, many refrigeration systems utilize mechanical compression, which is energy intensive. Nonetheless, there has been an increasing concern over conventional refrigeration system working fluids that contribute to ozone layer depletion, greenhouse effects, and global warming. One alternative to tackle these challenges is the development of more economic and environmentally sustainable refrigeration systems. Over the past decade, there has been an increasing interest in research to develop and improve absorption refrigeration systems (ARSs) [1]. An ARS is a feasible option for harnessing residual heat and renewable sources like solar and geothermal energy. Furthermore, the operating fluids of these processes are environmentally benign [2]. Though the global performance of the absorption cycle is usually poor – in terms of cooling effect per unit of supplied energy −, residual heat like the one rejected from power plants can be harnessed to improve the global energy utilization [3].

Ammonia-water (NH_3-H_2O) based systems are broadly employed where lower temperature levels are required. Nonetheless, water-lithium bromide (H_2O-LiBr) based systems are also extensively used where moderate temperature levels are required (for example, air-conditioning units), the latter system being more efficient than the former. Moreover, the environmental benefit of the ARSs using H_2O-LiBr as the refrigerant-absorbent working pair is already well-known. This advantage of H_2O-LiBr ARSs is not only over other refrigeration technologies such as vapor compression systems, but also over other ARSs using different working pairs such as NH_3-H_2O [4]. That is mainly because (i) ARS uses thermal energy instead of electricity, and (ii) to the best of our knowledge, the LiBr solution has no global warming or ozone depleting potential that has been reported in the open literature, satisfying the environmental criteria defined under both the Montreal and Kyoto Protocols. However, conventional single-effect ARSs show low energy efficiencies and they are limited to using heat sources of low

---

Nomenclature

Symbols

A_k	cost parameter for estimating investment for a process unit k ($/(ft^2)^{Bk}$) [Eq. (33)]
B_k	cost parameter for estimating investment for a process unit k (dimensionless) [Eq. (33)]
C_k	cost parameter for estimating investment for a process unit k ($) [Eq. (33)]
CAPEX	capital expenditures ($/yr)
CRF	capital recovery factor (dimensionless)
CU	cooling utility (t/yr)
$\mathbf{g}_t$	set of inequality constraints t
$\mathbf{h}_s$	set of equality constraints s
h_i	specific enthalpy of a process stream i (kJ/kg)
H_i	enthalpy flow rate of a process stream i (kW)
HTA_k	heat transfer area of a process unit k (m^2)
HU	heating utility (t/yr)
i	interest rate (dimensionless)
IN	subset of *PS* with the streams i entering a process unit k, except for utility streams (cooling water, chilled water, and hot source)
$LMTD_k$	logarithmic mean temperature difference in a process unit k (°C)
M_i	mass flow rate of a process stream i (kg/s)
n	project lifetime (yr)
OPEX	operating expenditures ($/yr)
OUT	subset of *PS* with the streams i leaving a process unit k, except for utility streams (cooling water, chilled water, and hot source)
P	pressure (kPa)
PC	set of the system components j
PS	set of the process streams i
PU	set of the process units k
Q_k	heat load in a process unit k; exchanged heat (kW)
T_i	temperature of a stream i (°C, K)
TAC	total annual cost ($/yr)

THTA	total heat transfer area of the system (m^2)
U_k	overall heat transfer coefficient for process unit k (kW/m^2/°C)
W_k	power in a process unit k (kW)
$\mathbf{x}$	vector of model variables
X_j	mass fraction of component j (% kg/kg)
Z_k	investment for a process unit k ($)

Greek letters

δ	a small positive value (parameter) used in model constraints Eqs. (13)−(29)
Δ	refers to the difference between two values
ε	effectiveness factor of a solution heat exchanger (dimensionless)

Subscripts

CU	cooling utility
HU	heating utility
i	a process stream
in	inlet
j	a system component
k	a process unit
min	minimum
out	outlet
s	an equality constraint of the mathematical optimization model
t	an inequality constraint of the mathematical optimization model
u	utility (cooling water, chilled water, and hot source)

Superscripts

C	cold side of a heat exchanger
H	hot side of a heat exchanger
L	lower bound

thermal levels [5] such as solar or geothermal energy sources, or low-grade residual heat from industrial processes. In order to enhance the ARS overall efficiency and overcome its limitation to heat source temperature, researchers have proposed improved configurations for ARS, including advanced configurations of multi-effect systems [6]. The double-effect ARS has attracted a lot of interest while being the most commercially applied multi-effect ARS [7].

Many researchers have dealt with the double-effect H_2O-LiBr ARS performing energy analyses, exergy analyses, and exergo-economic analyses. Kaushik and Arora [8] performed model-based parametric energy and exergy analyses of a series flow double-effect H_2O-LiBr ARS, and compared the results with a single-effect ARS. Particularly, they analyzed the effects of varying the generator, absorber, and evaporator temperatures, as well as the pressure drop between the evaporator and the absorber and the heat exchanger effectiveness, on the energetic and exergetic performance, in terms of the coefficient of performance, exergy destruction, efficiency defects, and exergetic efficiency. They also analyzed the effect of the temperature difference between the heat source and the generator, and between the evaporator and the cold room. Kaynakli et al. [9] performed a comparative energy and exergy analysis of a double-effect H_2O-LiBr ARS with series flow considering hot water, steam, and hot air as heat sources in the high-pressure generator. They carried out a parametric analysis of the operating temperatures on the coefficient of performance, exergy destruction in the high-pressure generator, heat capacity, and heat source mass flow

rate. Gomri [10] performed a simulation-based comparative analysis based on the first and second law of thermodynamics between single-effect and double-effect H_2O-LiBr ARSs for the same cooling specifications. The author studied the influence of the various operating parameters on the coefficient of performance, heat loads in the system's components, exergetic efficiency (rational efficiency), and the total exergy destruction associated with the two examined cycles. Talukdar and Gogoi [11] performed parametric energy and exergy analyses of a combined vapor power cycle and a double-effect H_2O-LiBr ARS as a bottoming cycle to evaluate its thermodynamic performance. They varied the temperature of the flue gas of the power cycle boiler which is the heat source for the high-temperature generator of the ARS. Also, they compared the energetic and exergetic performance of this process with the performance of a single-effect configuration for the same flue gas temperature. Morosuk and Tsatsaronis [12] proposed an advanced exergy analysis of energy conversion systems, which consists in splitting the total exergy destruction into endogenous/exogenous and unavoidable/avoidable parts. This splitting improves the accuracy of exergy analysis and the understanding of the thermodynamic inefficiencies, and facilitates the improvement of a system. They applied this development to an absorption refrigeration machine as an illustrative case study. An example of how this approach can be used to improve the design is shown in [13]. Garousi Farshi et al. [5] applied the exergo-economic method to analyze three types of double-effect H_2O-LiBr ARSs (series, parallel, and reverse parallel flow) at a broad

range of operating conditions. They investigated the effects of different thermodynamic parameters on the thermo-economic performance of the systems, i.e. the influence of various operating parameters on investment costs of the overall systems and product cost flow rates, and the contributions of component costs to the overall costs for each system. The overall heat transfer coefficient for each component was calculated at each operating condition since it constitutes a major criterion in cost forming processes. Misra et al. [14] applied the thermo-economic concept to the optimization of a double-effect H_2O-LiBr ARS system aimed at minimizing its overall economic cost of the product (i.e. the desired cooling effect). They applied a simplified cost minimization methodology based on the thermo-economic concept to calculate the economic costs of all the internal flows and products of the system by formulating thermo-economic cost balances. Once these costs are determined, the system is thermo-economically evaluated to identify the effects of the design variables on cost of the flows and products. This enables to suggest changes of the design variables that would make the overall system cost-effective. An approximate optimum design configuration can be obtained by means of an iterative procedure. Palacios Bereche et al. [15] performed a thermo-economic analysis of a double-effect H_2O-LiBr ARS by using the methodology of functional analysis with negentropy. The exergetic cost of the main product – the cooling cost – was calculated as a function of the exergy of the heat source. They analyzed two cases consisting of a direct-fired system and a steam-driven system as part of a cogeneration system.

One characteristic feature of the double-effect ARS is its ability to operate in parallel, series, and reverse parallel flow configurations according to the flow of the working solution through the heat exchangers and generators. Garousi Farshi et al. [7] studied, compared thermodynamically, and analyzed the advantages and disadvantages of series, parallel, and reverse parallel flow configurations of double-effect H_2O-LiBr ARSs with identical refrigeration capacities. Based on computational models developed in the EES software, they examined the influence of various operating parameters on the energetic and exergetic performance of the three configurations, and investigated the effects of component temperatures, the effectivenesses of the solution heat exchangers, pressure drops between the evaporator and the absorber and between the low-temperature generator and the condenser on their performance characteristics. Garousi Farshi et al. [16] studied and compared the effects of operating parameters on crystallization phenomena in the three mentioned configurations of double-effect H_2O-LiBr ARSs with identical refrigeration capacities. They showed that the range of operating conditions without crystallization risks in the parallel and the reverse parallel configurations is wider than those of the series flow system. Since low-grade waste heat can be supplied to the low-temperature generator, they also investigated the possibility of crystallization when this heat is supplied. Arun et al. analyzed the series flow [17] and parallel flow [18] double-effect H_2O-LiBr ARSs based on the concept of equilibrium temperature at the low-temperature generator – the temperature that results from the energy balance at the low-temperature generator for a set of operating parameters – which is used to estimate the system performance. The authors compared the coefficient of performance and its sensitivity to operating conditions for both flow cycles [18]. They showed that, for the examined range of operating conditions, the maximum attainable coefficient of performance for the parallel flow cycle is greater than that for the series flow cycle, and that the performance of the parallel flow system is more sensitive to the effectiveness of the low-temperature heat exchanger than that of the series flow configuration. External heat supplied to the low-pressure generator has greater impact on the parallel flow configuration than on the series flow configuration. Gebreslassie et al. [19] investigated different flow configurations (reverse, series, and parallel flow) of multi-effect H_2O-LiBr ARSs. They conducted an exergy analysis for single, double, triple, and half effect cycles considering only the unavoidable exergy destruction. The results represent the maximum attainable performance and are not affected by design specifications as,

for instance, UA values. They determined and compared the coefficient of performance, exergetic efficiencies, exergy destruction rates, and the effect of the heat source temperature for the different cycles and flow configurations applying the same methodology and assumptions.

The optimization of energy processes in general and ARS in particular by means of exergy-based methods is an iterative process. At present, the exergy-based methods may render that only a subset of the possible design solutions are considered [20]. Moreover, depending on available degrees of freedom in the optimization problem, these methods may require a considerable number of iterations and calculations [21] resulting in a computationally expensive solution. Process optimization based on exergo-economics is another approach for improving thermal systems combining exergy and economic analyses. Exergo-economic methods may be classified in two types: calculus and algebraic methods [22]. The latter methods use algebraic cost balance equations requiring proposing auxiliary cost equations for each component. The former methods use differential equations, where the cost flows of the system are obtained in conjunction with optimization procedures based on the Lagrange multiplier method, which determines marginal costs. In the calculus methods, the mathematical description of the function of each component is also subjective, which is one of the main weaknesses of the exergo-economic methods.

Systematic methods based on mathematical programming techniques have also been successfully applied to the optimization of other energy processes, especially for processes with a large number of degrees of freedom. Mussati et al. [23] presented a systematic optimization procedure for the synthesis and design of multi-stage flash-mixer (MSF) desalination processes, based on a superstructure model, aimed at minimizing the total annual cost for a desired water production. As a result, a new process configuration of the multi-stage flash-mixer system was obtained. Similarly, Druetta et al. [24] developed a nonlinear mathematical programming model of a multi-effect evaporation (MEE) system for seawater desalination for the same purposes. The relative marginal values corresponding to the optimal solution and a global sensitivity analysis were used to rank the process parameters according to their impacts on the total cost. Oliva et al. [25] applied the mathematical programming technique for the optimal synthesis and design of the heat exchanger network of the glycerol steam reforming process to produce hydrogen for proton-exchange membrane fuel cells (PEMFC) applications, while keeping the maximum attainable overall net energy efficiency of the integrated system, as determined in [26]. Serralunga et al. [27] proposed a modifier adaptation strategy for real-time optimization in a mathematical programming framework, which was applied to the heat and power system of a sugar and ethanol facility. These energy systems are suitable for being optimized in real-time because of their fast dynamics and the benefits achievable by reacting to changes in power prices and steam demand. Arias et al. [28] applied mathematical programming and superstructure-based optimization approaches to design multi-stage membrane systems for CO_2 capture, with the aim to systematically determine the optimal number of membrane stages, membrane areas, power requirements, the location of recycle streams, and operating conditions that satisfy desired CO_2 recovery-purity value pairs at a minimum total cost. Manassaldi et al. [29] developed a discrete and continuous nonlinear mathematical model based on a superstructure representation of a dual pressure heat recovery steam generator (HRSG) coupled to two steam turbines. They determined the optimal configuration and design by (i) maximization of the total net power generation for a given total heat transfer area, and (ii) minimization of the total heat transfer area for a required total net power generation. As a result, a HRSG configuration more efficient than a reference case reported by other authors was obtained. Then, the main advantage of using the mathematical programming techniques is that they allow a simultaneous optimization of all existing trade-offs among process variables. However, only few publications have dealt with mathematical programming approaches applied to the ARS optimization, in spite of the fact that the performance of the solvers

handling nonlinear constraints was greatly improved. Rubio-Maya et al. [30] presented a nonlinear mathematical programming model to optimize single-effect H_2O-LiBr ARSs by minimization of the annual cost. The model consists of a thermodynamic model based on the exergy concept, an economic model, and inequality constraints. They compared the obtained optimization results with those reported in other studies using a thermo-economic optimization method. Gebreslassie et al. [31] proposed a systematic method for the design of sustainable ARSs in a mathematical programming framework. The approach is based on a multi-objective formulation that simultaneously considers the minimization of total annual cost and environmental impact of the cycle at the design stage. They formulated a bi-criteria nonlinear programming problem, whose solution is defined by a set of Pareto points that represent the optimal trade-off between the economic and environmental targets. This approach offers a set of alternative options for system design rather than a single solution allowing to choose the best one according to other considerations.

This work is a follow-up to the work presented by Mazzei et al. [4] and Mussati et al. [32]. The equation-oriented mathematical optimization model, formulated as a NLP problem, of a single-effect H_2O-LiBr ARS presented by Mazzei et al. [4] is extended to a double-effect system with series flow configuration. This approach employs the cost model presented in Mussati et al. [32]. Compared to the single-effect system studied by Mazzei et al. [4], the double-effect configuration increases the degrees of freedom of the optimization problem and, consequently, the number of trade-offs that exist among the decision variables. Thus, the novelty of this paper is the simultaneous optimization of the trade-offs that exist among the operating conditions and the design (heat transfer area) of each process unit when the total annual cost (TAC) is minimized. This work differentiates itself from parametric simulation and parametric optimization studies on double-effect H_2O-LiBr ARSs previously mentioned in the literature. The resulting deterministic model simultaneously facilitates the achievement of optimal temperature, pressure, mass flow rate, and composition values of each process stream as well as the optimal heat transfer area values of the involved process units that lead to the minimal value of the TAC while meeting the target design specifications. In addition, the effectiveness factors of the solution heat exchangers are also considered as model variables as opposed to other published studies.

2. Process description

Fig. 1 shows a schematic of a conventional double-effect H_2O-LiBr ARS with series flow configuration studied by several researchers; for example by Garousi Farshi et al. [5] and Gomri and Hakimi [33]. It operates at three temperature levels: high, medium, and low level. The high-temperature generator (HTG) operates at high temperature, the low-temperature generator (LTG) and the condenser (COND) operate at medium pressure, and the evaporator (EVAP) and absorber (ABS) operate at low temperature level. The weak LiBr solution leaving the ABS is pumped to the HTG through the two heat exchangers: low-temperature solution heat exchanger (LTSHE) and high-temperature solution heat exchanger (HTSHE). A high-temperature heat source is used in the HTG to generate vapor from the weak solution. The strong solution leaving the HTG enters the LTG, through the HTSHE and the expansion valve EV3. In the LTG, the refrigerant (H_2O) vapor from the HTG condenses as a result of the low temperature of the strong LiBr solution, and its latent heat is used for producing water vapor from the strong solution. Apart from latent heat of condensation, low-grade thermal energy can also be harnessed to generate more vapor from this generator. Therefore, the strong solution increases its concentration and flows to the ABS through the LTSHE and the expansion valve EV2. The generated refrigerant vapor from both HTG and LTG enters the COND, transferring its condensation heat to the cooling utility as it condenses. Note that only the vapor generated in the HTG flows through the

expansion valve, EV4, before entering the COND. Afterwards, the liquid refrigerant flows to the EVAP through the valve EV1, which reduces its pressure to the operating pressure of the EVAP. The vapor leaving the EVAP enters the ABS, where it is dissolved in the strong solution from the LTG through the LTSHE and the expansion valve, EV2, rejecting its absorption heat to the cooling utility. This process is referred as double-effect ARS with "solution-to-HTG-first" series flow configuration.

3. Modeling

The mathematical model employed to determine the optimal design and operation conditions includes: equality constraints for describing the mass and energy balances of the process units, design relationships, and correlations for estimating the physicochemical and thermodynamic properties of the process streams, as well as inequality constraints to specify minimum allowable temperature difference approximations or avoid temperature crosses in the heat exchangers. The TAC is the objective function that is minimized.

3.1. Process model

The main model assumptions are the following:

- The system is at steady-state condition [34].
- Pressure drops are not considered in pipes and heat exchangers [19].
- Heat losses are not considered in the process units [34].
- The work by the solution pump is not considered in the total energy balance since it is negligible with respect to the heat loads in the process units [34].
- The refrigerant leaves the condenser and the evaporator at saturation conditions [19].
- The refrigerant leaves the low-temperature and high-temperature generators at superheated conditions [35].
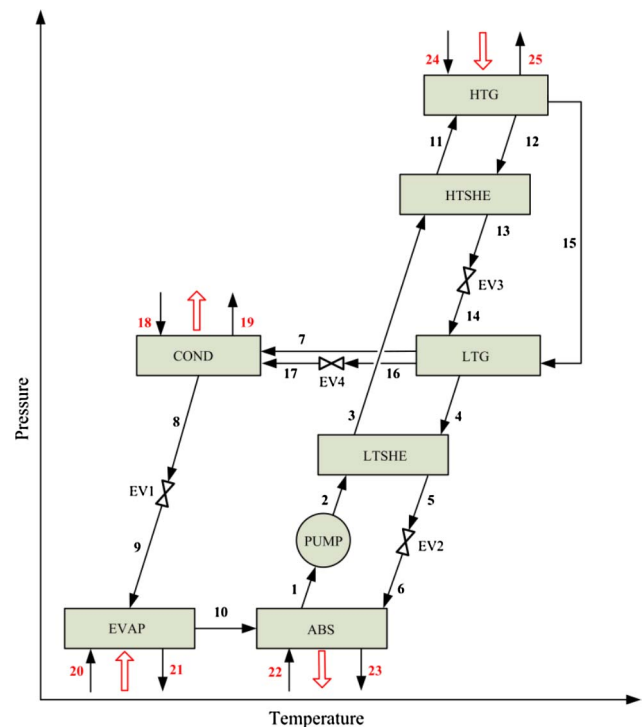- The weak LiBr solution leaves the absorber at saturated condition [16].

Fig. 1. Schematic of a double-effect H_2O-LiBr ARS with series flow (solution-to-HTG-first configuration).

- The strong LiBr solution leaves LTG and HTG at equilibrium at its corresponding pressure and temperature [16].
- All the expansion valves perform isenthalpic [34].

3.1.1. Definitions

Let *PU* be the set of the main process units vector *k*:

$$PU = \{ABS, HTG, LTG, COND, EVAP, HTSHE, LTSHE, EV1, EV2, EV3, EV4\} \tag{1}$$

Let *PS* be the set of the process streams vector *i*:

$$PS = \{1, \cdots i \cdots, 25\} \tag{2}$$

Let *PC* be the set of the system components vector *j*:

$$PC = \{LiBr, water, vapor\} \tag{3}$$

Let *IN* and *OUT* be the subsets of *PS* with the process streams entering and leaving the system, respectively. The following balances and relationships can now be formulated according to Fig. 1:

3.1.2. Mass and energy balances for a process unit k

Total mass balance:

$$\sum_{i \in IN} M_{i,k} - \sum_{i \in OUT} M_{i,k} = 0 , \forall k \in PU \tag{4}$$

Component mass balance:

$$\sum_{i \in IN} M_{i,k} \cdot X_{j,i,k} - \sum_{i \in OUT} M_{i,k} \cdot X_{j,i,k} = 0 , \forall k \in PU, j = LiBr \tag{5}$$

Energy balance:

$$Q_{u,k} - W_k + \sum_{i \in IN} H_{i,k} - \sum_{i \in OUT} H_{i,k} = 0 , \forall k \in PU$$

$$Q_{u,k} = \pm(H_{u,in,k} - H_{u,out,k}) \tag{6}$$

$$H_i = M_i \cdot h_i \tag{7}$$

M indicates mass flow rate (kg/s), *X* refers to mass fraction (kg/kg), *Q* is the heat load (kW), *W* refers to power (kW), *H* represents enthalpy flow rate (kW), and *h* is the specific enthalpy (kJ/kg).

3.1.3. Heat transfer area (HTA) of a process unit k

$$Q_k = U_k \cdot HTA_k \cdot LMTD_k , \forall k \in PU \tag{8}$$

Logarithmic mean temperature difference (LMTD) in process unit k:

$$LMTD_k = \frac{\Delta T_k^H - \Delta T_k^C}{\ln \frac{\Delta T_k^H}{\Delta T_k^C}} , \forall k \in PU \tag{9}$$

ΔT_k^H and ΔT_k^C are the temperature differences at the hot and cold sides, respectively.

Then, the total heat transfer area *THTA* (m²) is given by:

$$THTA = \sum_k HTA_k , \forall k \in PU \tag{10}$$

3.1.4. Effectiveness factor of the solution heat exchangers (SHE):

The effectiveness factor ε is based on the strong solution side, and it is calculated by Eqs. (11) and (12) for LTSHE and HTSHE, respectively:

$$\varepsilon_{LTSHE} = \frac{M_1 X_1 (T_3 - T_1)}{M_6 X_6 (T_4 - T_1)} \tag{11}$$

$$\varepsilon_{HTSHE} = \frac{M_3 X_3 (T_{11} - T_3)}{M_{12} X_{12} (T_{12} - T_3)} \tag{12}$$

3.1.5. Inequality constraints:

The following inequality constraints are included to avoid temperature crosses in the process units by assigning a small positive value to δ (in this case δ = 0.01):

High-temperature generator HTG:

$$T_{24} \geqslant T_{11} + \delta \tag{13}$$

$$T_{25} \geqslant T_{12} + \delta \tag{14}$$

High-temperature solution heat exchanger HTSHE:

$$T_{12} \geqslant T_{11} + \delta \tag{15}$$

$$T_{13} \geqslant T_3 + \delta \tag{16}$$

Low-temperature generator LTG:

$$T_{14} \geqslant T_4 + \delta \tag{17}$$

$$T_{15} \geqslant T_{14} + \delta \tag{18}$$

$$T_{15} \geqslant T_4 + \delta \tag{19}$$

$$T_{15} \geqslant T_{16} + \delta \tag{20}$$

Low-temperature solution heat exchanger LTSHE:

$$T_4 \geqslant T_3 + \delta \tag{21}$$

$$T_5 \geqslant T_2 + \delta \tag{22}$$

Absorber ABS:

$$T_{22} \geqslant T_{10} + \delta \tag{23}$$

$$T_6 \geqslant T_1 + \delta \tag{24}$$

$$T_6 \geqslant T_{23} + \delta \tag{25}$$

$$T_1 \geqslant T_{22} + \delta \tag{26}$$

Evaporator EVAP:

$$T_{20} \geqslant T_9 + \delta \tag{27}$$

$$T_{21} \geqslant T_9 + \delta \tag{28}$$

Condenser COND:

$$T_8 \geqslant T_{18} + \delta \tag{29}$$

3.1.6. Physico-chemical property estimation

The model includes correlations to compute the physicochemical properties of the process streams (strong and weak LiBr solutions, water, and vapor). The LiBr solution enthalpy at 40–70% concentration range is estimated by the correlation proposed by ASHRAE [36]. The crystallization conditions of the LiBr solution are considered using the correlation given by Boryta et al. [37]. Water and vapor properties are estimated through correlations given by Rogers and Mayhew [38].

The parameters used for optimization are listed in Table 1. The main

Table 1
Process data.

Parameter	Value
Cooling capacity (kW)	300.00
Inlet temperature (°C)	
Cooling water in the condenser, T_{18}	25.00
Cooling water in the absorber, T_{22}	25.00
Chilled water in the evaporator, T_{20}	13.00
Hot source in the HT generator, T_{24}	131.00
Heat transfer coefficient (kW/m²/°C)	
Evaporator, U_{EVAP}	1.50
Absorber, U_{ABS}	0.70
Condenser, U_{COND}	2.50
LT/HT generators, U_{LTG}/U_{HTG}	1.50
LT/HT heat exchangers, U_{LTSHE}/U_{HTSHE}	1.00

Table 2
Lower and upper bounds on optimization variables.

Variable	Lower bound	Upper Bound
LiBr concentration (%)	40.00	70.00
Pressure of refrigerant and LiBr solution streams (kPa)	0.10	15.00
Mass flow rate of refrigerant and LiBr solutions (kg/s)	0.00	100.00

Table 3
Parameter values for estimating process unit investment Z_k (see Eq. (33)).

Unit k	A_k	B_k	C_k
GEN	1800	0.8	24,915
EVAP	5900	0.552	0
ABS	9.976	1.820	0
COND	2119	0.497	0
SHE	2674	0.465	0

Table 4
Comparison of the simulated operating condition values predicted by the proposed model (SimSol) and the values reported by Garousi Farshi et al. [16].

Stream #	Temperature (°C)		Mass flow rate (kg/s)		Solution conc. (mass fraction, % LiBr, kg/kg of sol.)	
	Ref. [16]	SimSol	Ref. [16]	SimSol	Ref. [16]	SimSol
1	35.0	35.0	1.735	1.738	55.880	55.900
2	35.0	35.0	1.735	1.738	55.880	55.900
3	62.5	61.4	1.735	1.738	55.880	55.900
4	80.0	79.0	1.608	1.610	60.294	60.316
5	48.7	50.0	1.608	1.610	60.294	60.316
6	48.7	50.0	1.608	1.610	60.294	60.316
7	80.00	79.0	0.062	0.062	–	–
8	35.0	34.9	0.127	0.127	–	–
9	4.0	4.0	0.127	0.127	–	–
10	4.0	4.0	0.127	0.127	–	–
11	106.8	105.2	1.735	1.738	55.880	55.900
12	130.0	130.0	1.670	1.672	58.070	58.087
13	83.9	80.9	1.670	1.672	58.070	58.087
14	83.9	80.9	1.670	1.672	58.070	58.087
15	130.0	130.0	0.065	0.065	–	–
16	82.5	82.5	0.065	0.065	–	–
17	35.0	34.9	0.065	0.065	–	–

Table 5
Comparison of the simulated heat loads in the main process units predicted by the proposed model (SimSol) and the values reported by Garousi Farshi et al. [16].

Unit	Heat load (kW)		Deviation (%)
	Ref. [16]	SimSol	
EVAP	300.000	300.00	0
GEN	252.445	255.590	1.246
COND	167.213	167.590	0.225
ABS	385.241	388.000	0.716

decision variables considered for optimization are temperature, pressure, composition, and flow rate of all streams. Upper and lower bounds of the main process variables are listed in Table 2.

3.2. Cost model

The total annual cost (*TAC*) is calculated using Eq. (30). This calculation takes into account the total capital expenditures (*CAPEX*) and the total operating expenditures (*OPEX*):

$$TAC = CAPEX + OPEX \tag{30}$$

In Eq. (30), *CAPEX* is calculated using Eq. (31) in terms of the capital recovery factor (*CRF*) and the investment (Z_k) for each process unit k, which are calculated using Eq. (32) and Eq. (33), respectively. The *CRF* is computed for an assumed project lifetime (*n*) of 25 years and an interest rate (*i*) of 10.33% [32].

$$CAPEX = CRF \cdot \sum_k Z_k \tag{31}$$

$$CRF = \frac{i \cdot (1+i)^n}{(1+i)^n - 1} \tag{32}$$

$$Z_k = A_k \cdot (f \cdot HTA_k)^{B_k} + C_k \tag{33}$$

In Eq. (33), the investment Z_k is expressed in \$ and HTA_k in m²; the coefficient $f = 10.764 \, \text{ft}^2/\text{m}^2$ is the area conversion factor; and the numerical values of parameters A_k (\$/(ft²)^{Bk}), B_k (dimensionless), and C_k (\$) are listed in Table 3 [39].

The *OPEX* is calculated using Eq. (34). This equation includes costs associated with the heating (*HU*) and cooling (*CU*) utilities. The individual unit costs are $C_{HU} = 3.0$ \$/t and $C_{CU} = 0.0195$ \$/t [32].

$$OPEX = C_{HU} \cdot HU + C_{CU} \cdot CU \tag{34}$$

3.3. Optimization model

The optimization problem consists of minimizing the total annual cost *TAC* – calculated using Eq. (30) − for a required (fixed) cooling capacity, which is formally expressed as follows:

$Minimize \, TAC$
$s.t.$:
$$\begin{cases} \mathbf{h}_s(\mathbf{x}) = 0 \, , \, \forall \, s \\ \mathbf{g}_t(\mathbf{x}) \leqslant 0 \, , \, \forall \, t \\ Q_{\text{EVAP}} = 300 \, \text{kW} \\ \varepsilon_{\text{LTSHE}} \geqslant \varepsilon_{\text{SHE}}^L = 0.5 \\ \varepsilon_{\text{HTSHE}} \geqslant \varepsilon_{\text{SHE}}^L = 0.5 \end{cases} \tag{35}$$

where $\mathbf{x}$ is the vector of model variables; $\mathbf{h}_s(\mathbf{x})$ refers to equality constraints given by Eqs. (4)-(12), which include the mass and energy balances, correlations for physicochemical properties estimation, design specifications, and cost estimation; and $\mathbf{g}_t(\mathbf{x})$ refers to inequality constraints which are employed to avoid temperature crosses in the process units (Eqs. (13)-(29)) and to impose lower and/or upper bounds on a few critical operating variables. Particularly, a lower bound value ($\varepsilon^L_{\text{SHE}} = 0.5$) is imposed on the effectiveness factors (ε) of the solution heat exchangers LTSHE and HTSHE given by Eqs. (11) and (12), respectively. Finally, the required cooling capacity in EVAP (Q_{EVAP}) is 300 kW.

The proposed optimization problem aims at obtaining:

– Minimal TAC and its optimal distribution between CAPEX and OPEX.
– Optimal sizes (heat transfer areas) of the process units.
– Optimal values of temperature, pressure, composition, and flow rate of all process streams.

The derived NLP model involves 190 variables and 215 (equality and inequality) constraints. The inequality constraints are included to facilitate the model convergence by avoiding, for instance, temperature crosses in heat exchangers. The model was implemented in the General Algebraic Modeling System GAMS v. 23.6.5 [40], which is a high-level modeling tool for mathematical programming and optimization, and solved employing the solver CONOPT 3 v. 3.14W [41], which is a local optimizer that uses a feasible-path method based on the generalized reduced gradient (GRG) algorithm. Since CONOPT is a local search optimization algorithm, obtaining global optimal solutions cannot be
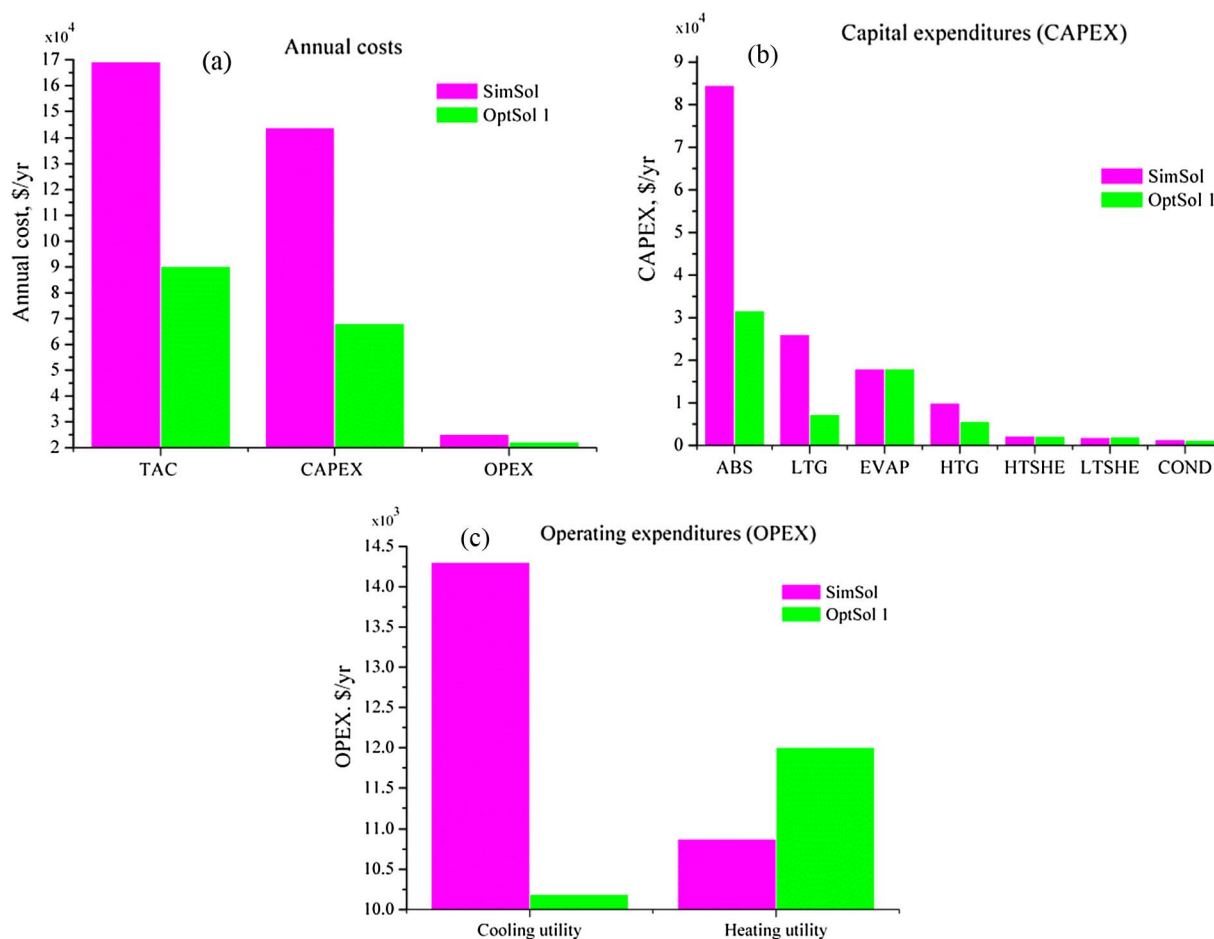
Fig. 2. Cost comparison between the test-bed (simulated) solution SimSol and the optimal solution OptSim 1 which applies a lower bound value of 0.5 for the effectiveness factor of the solution heat exchangers LTSHE and HTSHE: (a) annual costs, (b) CAPEX for each process unit, (c) OPEX for each utility.

mathematically guaranteed due to the non-convex nature of the model. However, numerous model executions starting from different initialization points lead to the same optimal solution, which should give confidence in the obtained optimal solution. The initial guess values were proposed based on the insights gathered from the optimization of the single-effect H_2O-LiBr ARS configuration [4] as well as on simulation results for the double-effect configuration reported in the literature [16].

4. Results and discussion

First, the proposed process model is verified by comparison of simulation outputs with literature values. Then, the model is employed for optimization purposes.

4.1. Model verification

The first step for model verification is to ensure that the implementation of the proposed NLP mathematical model is correct. This is mainly to check the accuracy of the model outputs; hence, a set of values corresponding to a case study presented in Garousi Farshi et al. [16] for a double-effect H_2O-LiBr ARS are used as a benchmark case study for verification, through comparison of the model predictions obtained with our model with their results. To this end, it is necessary to assign values to a set of model variables. For example, some degrees of freedom can be fixed in order to reproduce the solution provided in Garousi Farshi et al. [16]. The operating conditions of the main process streams (refrigerant, weak and strong LiBr solutions represented by streams #1 to #17 in Fig. 1) and the heat load in each process unit were

compared. Note that streams related to cooling and heating utilities (streams #18 to #25 in Fig. 1) were not considered in the comparison with the study of Garousi Farshi et al. [16] since they are not needed to close the overall energy balance of the system. Thus, in this case the model is used as a simulator or test-bed instead of an optimizer and the resulting simulated solution is hereafter named as "SimSol".

Tables 4 and 5 compare the operating conditions of each process stream (temperature, mass flow rate, and solution concentration) and the heat load in each process unit, respectively, for the configuration shown in Fig. 1. The comparison shows there is a good agreement between the predicted values (SimSol) and the reported values of Garousi Farshi et al. [16].

4.2. Minimization of the total annual cost

Once the double-effect ARS model is successfully verified, it is employed for optimization purposes. Therefore, the variables which were assigned fixed values in the model verification step (see above), are now set free, and are considered as optimization variables. Moreover, a lower bound value of 0.5 for the effectiveness factor of the solution heat exchangers LTSHE and HTSHE was imposed (Eqs. (11) and (12), respectively). The minimization of the TAC, which includes the CAPEX and OPEX, was used as the objective function. The obtained optimal solution is hereafter named "OptSol 1". The employed cost model is given by Mussati et al. [32], and is also provided in Section 3.2.

Figs. 2 and 3, as well as Table 6, compare the optimal solution OptSol 1 with the test-bed solution SimSol. Fig. 2a compares the TAC, CAPEX, and OPEX values; Fig. 2b and 2c compare the individual
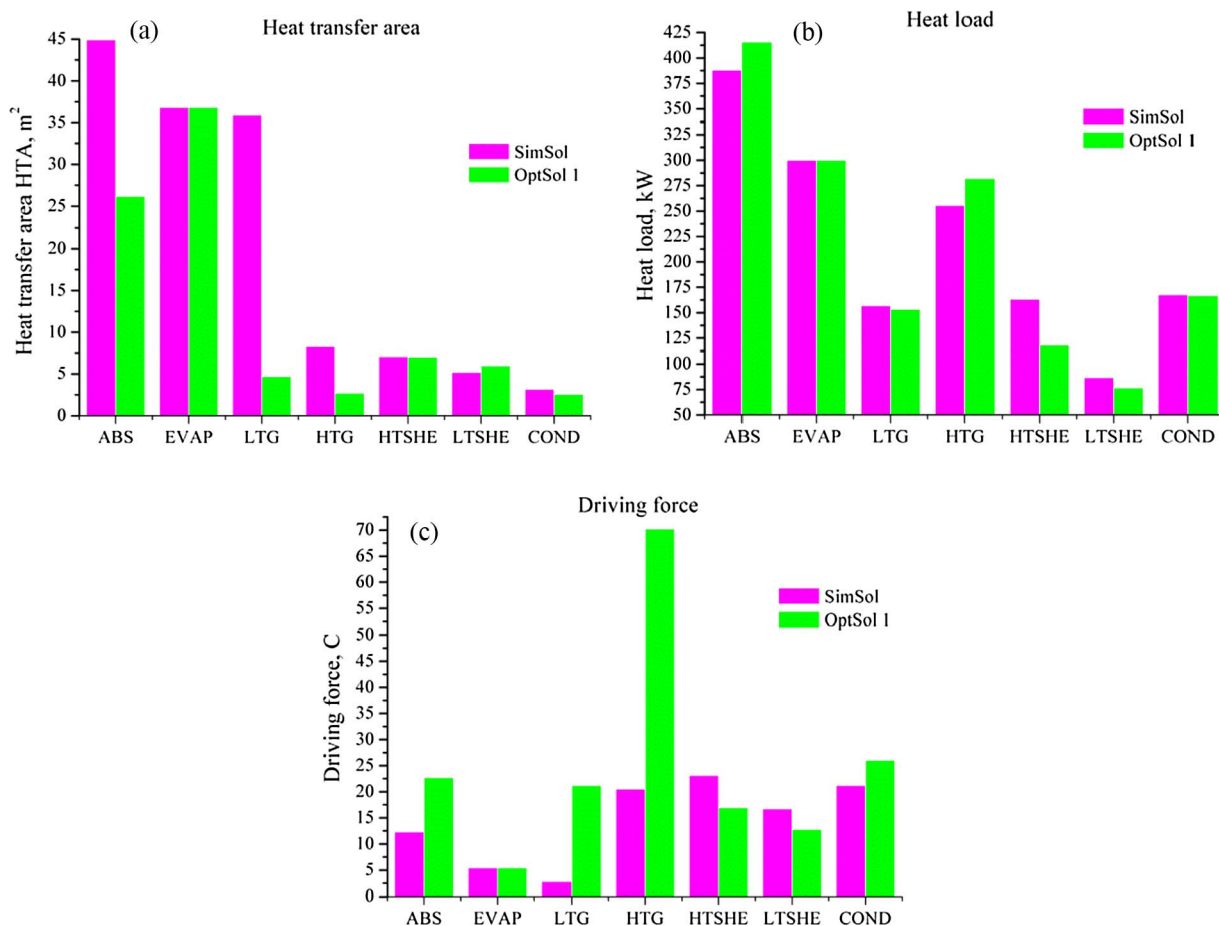
Fig. 3. Comparison between the test-bed (simulated) solution SimSol and the optimal solution OptSol 1: (a) HTA, (b) heat load, (c) driving force, in each process unit.

Table 6
Comparison of the operating conditions between the simulation output SimSol and the optimal solution OptSol 1.

Stream #	Temperature (°C)		Pressure (kPa)		Mass flow rate (kg/s)		Solution conc. (mass fraction,% LiBr, kg/kg of sol.)	
	SimSol	OptSol 1	SimSol	OptSol 1	SimSol	OptSol 1	SimSol	OptSol 1
1	35.0	47.2	0.814	0.814	1.738	3.048	55.900	62.131
2	35.0	47.2	52.400	90.00[a]	1.738	3.048	55.900	62.131
3	61.4	60.6	52.400	90.00[a]	1.738	3.048	55.900	62.131
4	79.0	74.1	5.620	7.115	1.610	2.920	60.316	64.895
5	50.0	59.5	5.620	7.115	1.610	2.920	60.316	64.895
6	50.0	59.5	0.814	0.814	1.610	2.920	60.316	64.895
7	79.0	74.1	5.620	7.115	0.062	0.061	–	–
8	34.9	39.2	5.620	7.115	0.127	0.128	–	–
9[b]	4.0	4.0	0.814	0.814	0.127	0.128	–	–
10[b]	4.0	4.0	0.814	0.814	0.127	0.128	–	–
11	105.2	81.4	52.400	90.00[a]	1.738	3.048	55.900	62.131
12	130.0	98.7	52.400	90.00[a]	1.672	2.980	58.087	63.537
13	80.9	77.1	52.400	90.00[a]	1.672	2.980	58.087	63.537
14	80.9	77.1	5.620	7.115	1.672	2.980	58.087	63.537
15	130.0	98.7	52.400	90.00[a]	0.065	0.067	–	–
16	82.5	96.7	52.400	90.00[a]	0.065	0.067	–	–
17	34.9	39.2	5.620	7.115	0.065	0.067	–	–
18	25.0	25.0	101.00	101.00	5.036	2.912	–	–
19	33.0	38.7	101.00	101.00	5.036	2.912	–	–
20[b]	13.0	13.0	101.00	101.00	12.019	12.019	–	–
21[b]	7.0	7.0	101.00	101.00	12.019	12.019	–	–
22	27.0	27.0	101.00	101.00	18.654	13.963	–	–
23	32.0	34.1	101.00	101.00	18.654	13.963	–	–
24	131.0	131.0	278.44	278.44	0.117	0.129	–	–
25	131.0	131.0	278.44	278.44	0.117	0.129	–	–

[a] Variable value reached the upper bound.

[b] Identical values in both solutions as a consequence of the problem specification (required cooling capacity, evaporator operating temperature, and the inlet and outlet temperatures of the stream to be cooled).

Table 7
Comparison of costs between the optimal solutions OptSol 1 and OptSol 2.

Cost ($/yr)	OptSol 1	OptSol 2	Variation (%)
TAC	90239.92	81632.21	−9.5
CAPEX	68047.70	60517.67	−11.1
LTSHE	2043.08	4.36	−99.8
HTSHE	2202.58	1735.31	−21.2
HTG	5673.83	7010.53	23.5
LTG	7299.70	7492.17	2.6
ABS	31623.89	25103.13	−20.6
COND	1215.51	1183.07	−2.67
EVAP	17989.10	17989.10	0
OPEX	22192.27	21114.54	−4.86
Cooling utility	10187.86	8154.07	−20.0
Heating utility	12004.37	12960.47	8.0

contributions of each cost item to the CAPEX and OPEX, respectively. Fig. 3 depicts the comparison between the values of HTA (3a), heat load (3b), and driving force (3c); and Table 6 presents the operating conditions (stream temperature, pressure, mass flow rate, and concentration).

The information presented in Fig. 2a reveals that the simultaneous optimization allowed reducing the TAC by nearly 46.7%, from 169243.91 $/yr. (SimSol) to 90239.92 $/yr. (OptSim 1). This reduction takes place because the CAPEX is decreased by 52.8% (144068.03 vs. 68047.70 $/yr) and the OPEX is decreased by 11.8% (25175.88 vs. 22192.27 $/yr). Fig. 2b shows that the investment costs of the process units decreased considerably, except for HTSHE which is decreased by only 0.23%. The investment cost for LTSHE, as opposed to the rest of the units, is increased by 6.8% (1913.36 vs. 2043.08 $/yr.) due to an increase by 0.78 m^2 in its HTA (Fig. 3a). In fact, the investment cost of LTG decreased by around 72.0% (Fig. 2b) because its HTA decreased from 35.91 to 4.66 m^2 (87%), while the investment cost of the high-temperature generator HTG decreased by 43.1% due to a reduction of its HTA of 67.7% (from 8.30 to 2.68 m^2). The investment cost for ABS decreased by around 62.6%, as a consequence of the reduction in the HTA by 41.7%. COND showed a reduction in investment cost by around 10.0% due to a reduction of its area by 19.1% which is not as significant as for the two generators and the absorber. The investment cost of EVAP is the same in both solutions due to the definition of identical specifications in both problems (the required cooling capacity, evaporator operating temperature, and the inlet and outlet temperatures of the stream to be cooled).

Fig. 3a shows that the reductions of the HTA for different process units computed by OptSol 1 are mainly due to increases in driving forces (Fig. 3c) resulting from modifications in operating conditions of the involved process streams. This is also indicated in Table 6. In this regard, it is worth mentioning that the process units are highly interrelated and that a variation of one or more variables in a process unit determines a variation of one or more variables of the remaining units. For instance, for almost the same heat load values predicted for the LTG
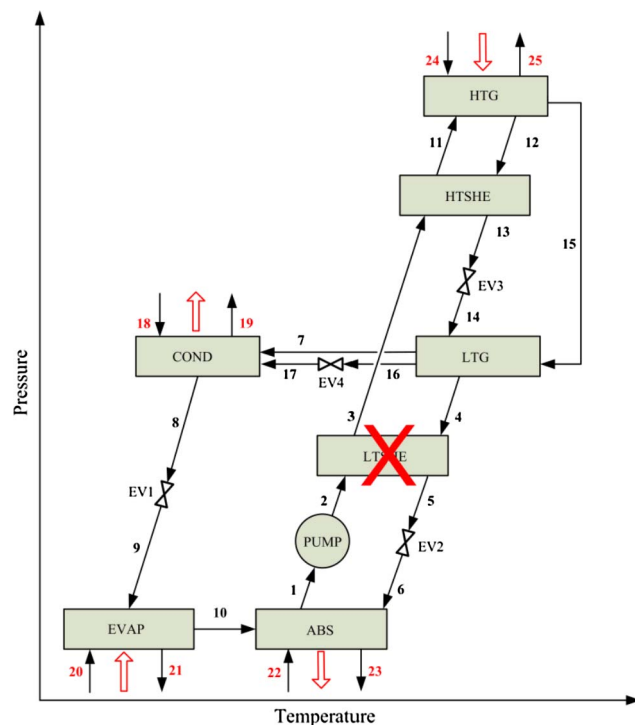

Fig. 4. Schematic of a new double-effect H$_2$O-LiBr ARS with series flow obtained by minimization of the TAC (OptSol 2).

by both solutions (156.785 kW by SimSol and 153.092 kW by OptSol 1, Fig. 3b), the driving force is increased from 2.8 °C to 21.2 °C (Fig. 3c). This is because of a 31.3 °C temperature decrease in stream #15 due to a 37.6 kPa pressure increase and a 6.231% solution concentration increase in stream #11 and a 5.45% concentration increase in stream #12 –see Table 6.

On the other hand, the temperature of stream #16 (liquid at saturation condition) increased from 82.5 to 96.7 °C. However, the temperature of stream #4 is decreased by 4.9 °C (from 79.0 to 74.1 °C) due to an increase in (i) its pressure from 5.620 to 7.115 kPa, (ii) its composition from 60.316 to 64.895% LiBr, and (iii) its mass flow rate from 1.610 to 2.920 kg/s. Thus, the OptSol 1 solution results in the reduction of the LTG area by 87%, compared to the area calculated for the SimSol result.

Regarding the HTG, Fig. 3 shows that an increase of the driving force from 20.5 to 70.2 °C allowed not only to decrease the HTA by 5.62 m^2 with respect to SimSol (8.30 vs. 2.68 m^2) but also to increase the heat load by 26.568 kW (255.590 vs. 282.158 kW). The increase of the driving force is due to the decrease in temperature of streams #11 (105.2 vs. 81.4 °C) and #12 (130.0 vs. 98.7 °C). Such decreases are possible due to the pressure increase from 52.4 to 90.0 kPa in both streams, the increase of the flow rate and composition of stream #11

Table 8
Comparison of heat transfer area, heat load, and driving force values in each process unit between optimal solutions OptSol 1 and OptSol 2.

Unit	Heat transfer area, HTA (m^2)		Heat load (kW)		Driving force (°C)	
	OptSol 1	OptSol 2	OptSol 1	OptSol 2	OptSol 1	OptSol 2
ABS	26.16	23.04	415.532	440.047	22.7	27.3
LTSHE	5.96 ($\varepsilon_{LTSHE} = 0.5^a$)	0.0000108 ($\varepsilon_{LTSHE} = 0.000306$)	76.431	0.000306	12.8	28.5
LTG	4.66	4.91	153.092	158.188	21.2	20.8
HTSHE	7.01 ($\varepsilon_{HTSHE} = 0.545$)	4.2 ($\varepsilon_{HTSHE} = 0.533$)	118.178	138.118	16.9	32.9
HTG	2.68	4.29	282.158	304.631	70.2	47.3
COND	2.56	2.43	166.626	164.584	26.0	27.1
EVAP	36.83	36.83	300.00	300.00	5.4	5.4

[a] Variable value reached the upper bound.

Table 9
Comparison of the operating conditions between the optimal solutions OptSol 1 and OptSol 2.

| Stream #	Temperature (°C)		Pressure (kPa)		Mass flow rate (kg/s)		Solution conc. (mass fraction, % LiBr, kg/kg of sol.)	
	OptSol 1	OptSol 2	OptSol 1	OptSol 2	OptSol 1	OptSol 2	OptSol 1	OptSol 2
1	47.2	46.0	0.814	0.814	3.048	1.864	62.131	61.512
2	47.2	46.0	90.00[a]	90.00[a]	3.048	1.864	62.131	61.512
3	60.6	46.0	90.00[a]	90.00[a]	3.048	1.864	62.131	61.512
4	74.1	74.5	7.115	7.571	2.920	1.735	64.895	66.066
5	59.5	74.5	7.115	7.571	2.920	1.735	64.895	66.066
6	59.5	74.5	0.814	0.814	2.920	1.735	64.895	66.066
7	74.1	74.5	7.115	7. 571	0.061	0.060	–	–
8	39.2	40.4	7.115	7. 571	0.128	0.128	–	–
9	4.0	4.0	0.814	0.814	0.128	0.128	–	–
10	4.0	4.0	0.814	0.814	0.128	0.128	–	–
11	81.4	85.2	90.00[a]	90.00	3.048	1.864	62.131	61.512
12	98.7	119.6	90.00[a]	90.00	2.980	1.795	63.537	63.856
13	77.1	77.5	90.00[a]	90.00	2.980	1.795	63.537	63.856
14	77.1	77.5	7.115	7.571	2.980	1.795	63.537	63.856
15	98.7	119.6	90.00[a]	90.00	0.067	0.068	–	–
16	96.7	96.8	90.00[a]	90.00	0.067	0.068	–	–
17	39.2	40.4	7.115	7.571	0.067	0.068	–	–
18	25.0	25.0	101.00	101.0	2.912	2.652	–	–
19	38.7	39.9	101.00	101.0	2.912	2.652	–	–
20	13.0	13.0	101.00	101.0	12.019	12.019	–	–
21	7.0	7.0	101.00	101.0	12.019	12.019	–	–
22	27.0	27.0	101.00	101.0	13.963	10.855	–	–
23	34.1	36.7	101.00	101.0	13.963	10.855	–	–
24	131.0	131.0	278.44	278.44	0.129	0.140	–	–
25	131.0	131.0	278.44	278.44	0.129	0.140	–	–

[a] Variable value reached the upper bound.
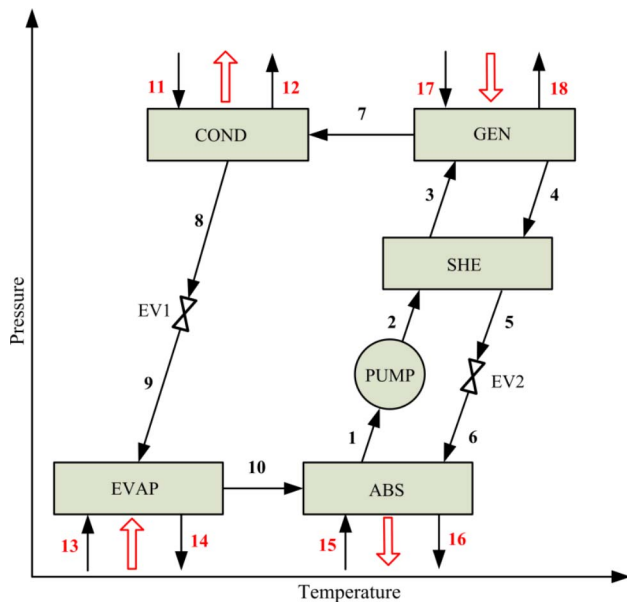
Fig. 5. Schematic of a conventional single-effect H_2O-LiBr ARS.

from 1.738 to 3.048 kg/s and from 55.900% LiBr to 62.131% LiBr, respectively, and of stream #12 from 1.672 to 2.980 kg/s, as well as from 58.087 to 63.537% LiBr, respectively (Table 6).

The same behavior of the HTG can be observed for the ABS by comparing the values of the HTA, heat loads, and driving forces, which are shown in Fig. 3. In this unit, the driving force increases due to the increase of the temperature and concentration of stream #1 (by 12.2 °C and 6.231% LiBr, respectively), and stream #6 (by 9.5 °C and 4.579% LiBr, respectively) since all the streams involved in the ABS are at the operating pressure of 0.814 kPa in both the SimSol and OptSol 1 solutions.

Although the heat load in the exchanger LTSHE computed by OptSol

1 is lower than SimSol (76.431 vs. 86.614 kW), the area is slightly higher (5.96 vs. 5.18 m²) because the driving force is 3.9 °C lower. Regarding the heat exchanger HTSHE, the required area is practically the same (around 7 m²) even though the heat transferred in OptSol 1 is 44.874 kW lower than in SimSol, but implying a driving force of 16.9 °C compared to 23.1 °C required in SimSol.

With respect to the operating expenditures OPEX, Fig. 2c shows that the heating utility cost computed by OptSol 1 increased by 10.4% (from 10874.00 to 12004.37 $/yr) but the cooling utility cost decreased by 28.8% (14301.88 vs. 10187.86 $/yr), which led to a (total) OPEX decrease of about 11.8% (25175.88 vs. 22192.27 $/yr).

However, the optimal solution OptSol 1 for the optimization problem formulated in Eq. (35) reported in Table 6 indicates that the value of the effectiveness factor of the heat exchanger LTSHE ε_{LTSHE} (Eq. (11)) reached the imposed lower bound value $\varepsilon_{SHE}^L = 0.5$, unlike the optimal value calculated for HTSHE ε_{HTSHE} (Eq. (12)), which was 0.545. In this regard, it is important to mention that the effectiveness factors of heat exchangers ε are considered as optimization variables instead of fixed model parameters. Therefore it is interesting to investigate how the optimal solution OptSol 1 modifies when the optimization problem given by Eq. (35) is solved by setting a lower bound $\varepsilon_{SHE}^L = 1 \cdot 10^{-7}$ to ε_{LTSHE} and ε_{HTSHE} instead of 0.5, i.e. when the optimization problem given by Eq. (36) is solved. From a practical point of view, these settings mean that essentially no lower bound is imposed, but providing a value different from zero to these constraints is necessary from a numerical solution strategy point of view to avoid potential division by zero and, consequently, to facilitate the model convergence.

Minimize TAC
s.t. :
$$\begin{cases} \mathbf{h}_s(\mathbf{x}) = 0 \text{ , } \forall \text{ } s \\ \mathbf{g}_t(\mathbf{x}) \leqslant 0 \text{ , } \forall \text{ } t \\ Q_{EVAP} = 300 \text{ kW} \\ \varepsilon_{LTSHE} \geqslant \varepsilon_{SHE}^L = 1 \cdot 10^{-7} \\ \varepsilon_{HTSHE} \geqslant \varepsilon_{SHE}^L = 1 \cdot 10^{-7} \end{cases}$$

(36)

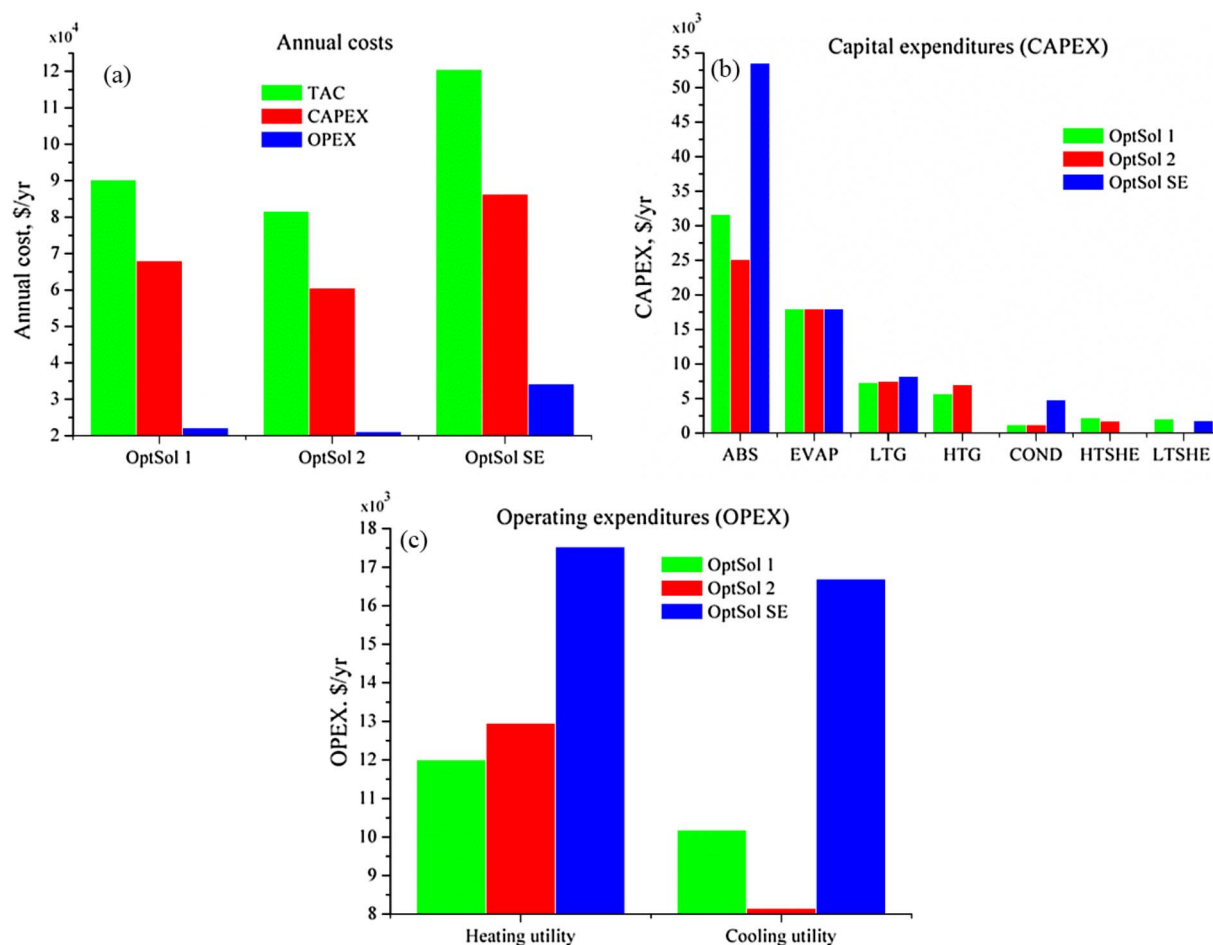The optimal solution obtained for the cost optimization problem

Fig. 6. Comparison among the optimal solutions for the double-effect configuration (OptSol 1 and OptSol 2) and the single-effect configuration (OptSol SE): (a) annual cost, (b) CAPEX for each process unit, (c) OPEX for each utility.

(36) is named OptSol 2 and is compared to OptSol 1 in detail in the next section.

4.3. Comparison of the optimal solutions OptSol 1 and OptSol 2

Table 7 compares the minimal TAC values and the individual contribution of the cost items to the CAPEX and OPEX values obtained by OptSol 1 and OptSol 2. The minimal TAC obtained by OptSol 2 is 9.5% lower than the obtained by OptSol 1 since CAPEX and OPEX decreased by 11.1% and 4.86%, respectively, while Table 8 compares the HTA, heat load, and driving force values in each process unit between OptSol 1 and OptSol 2.

It can be observed that the optimal solution OptSol 2 eliminates the low-temperature heat exchanger LTSHE from the configuration since its HTA is negligible ($1.08 \cdot 10^{-5} \, m^2 \approx 0 \, m^2$). This is a consequence of the changing of the lower bound value ε_{SHE}^L imposed to the heat exchanger effectiveness factors from 0.5 to $1 \cdot 10^{-7}$. The resulting optimal value of ε_{LTSHE} is $3.06 \cdot 10^{-6}$; it does not reach the lower bound $\varepsilon_{SHE}^L = 1 \cdot 10^{-7}$ due to the constraints on the temperature of the process streams involved in LTSHE that become active (Eqs. (21) and (22)); as far as these constraints are relaxed by diminishing δ, ε_{LTSHE} approaches the imposed lower bound $\varepsilon_{SHE}^L = 1 \cdot 10^{-7}$. On the other hand, the optimal ε_{HTSHE} value for HTSHE results to be 0.533 (Table 8), which is an indication that it is needed in the resulting process configuration with a HTA of $4.2 \, m^2$. This process configuration resulting from OptSol 2 which is schematized in Fig. 4 has not been reported in the literature to the best of our knowledge.

Apart from changes on the operating conditions of most process

streams, the elimination of LTSHE determines not only a significant decrease of the investment cost of the total transfer area for heat exchangers (59%) but also for the absorber ABS (20.6%), and to a minor extent for the condenser COND (2.67%). However, these decreases imply an increase of the investment cost for the HTG of 23.5% and for the LTG of 2.6% due to the increase of their HTA values by 60.1% and 5.3%, respectively (Table 8). These variations in the sizes of the process units also require changes of the operation conditions. For example, they determine an increase of the heat load by 8.0% and 3.3% for the HTG and LTG, respectively, which imply an increase of the heating utility flow rate from 0.129 to 0.140 kg/s (stream #24 in Table 9) with an associated heating cost that is 8.0% greater for OptSol 2 than for OptSol 1 (12004.37 $/yr. for OptSol 1 vs. 12960.47 $/yr. for OptSol 2). Table 9 shows that the greatest temperature change corresponds to stream #12, where temperature increases from 98.7 to 119.6 °C. The results also indicate that all process streams, except streams #15 (and consequently #16 and #17) and #24 (and consequently #25) decrease their mass flow rates in OptSol 2 compared to OptSol 1. Finally, it should be mentioned that the solution concentration values also change; the concentration in stream #1 (and consequently in #2, #3, and #11) decreases slightly from 62.131 to 61.512% LiBr; in stream #4 (and consequently in #5 and #6) the concentration increases from 64.895 to 66.066% LiBr; and in stream #12 (and consequently in #13 and #14) it increases very slightly from 63.537 to 63.856% LiBr.

Finally, the optimization problem – TAC minimization – was solved by varying parametrically the values of the cooling capacity (Q_{EVAP}) from 150 to 450 kW and the temperature of the cooling water required in the COND (T_{18}) and ABS (T_{22}) from 15 to 35 °C, but keeping the
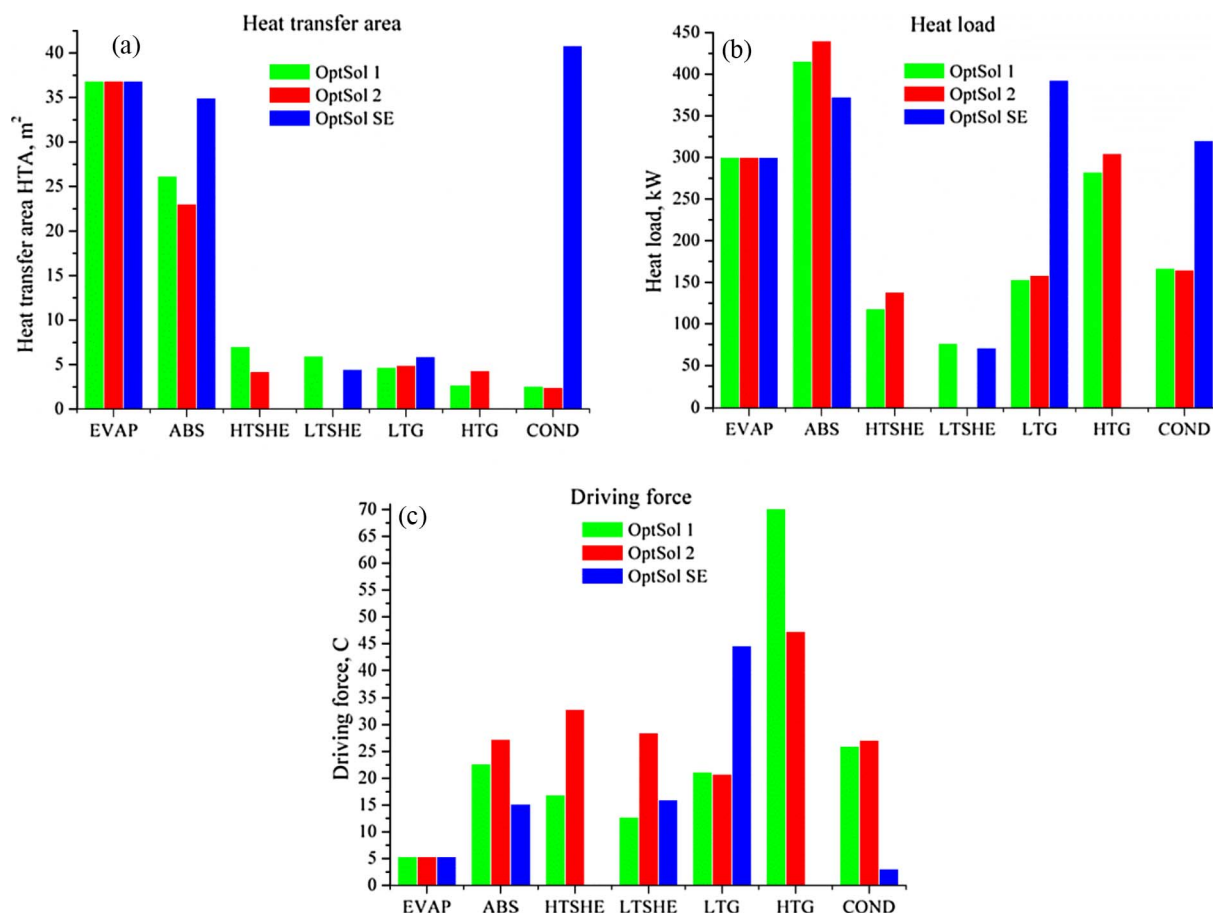
Fig. 7. Comparison among the optimal solutions for the double-effect configuration (OptSol 1 and OptSol 2) and the single-effect configuration (OptSol SE): (a) heat transfer area, (b) heat load, and (c) driving force, in each process unit.

Table 10
SWOT analysis.

Strengths	Weaknesses
– Nonlinear mathematical programming modeling allows optimizing the multi-effect ARSs – TAC minimization allows obtaining a structure of the double-effect ARS with series flow that has not been reported in the literature, where the LTSHE is eliminated from the conventional structure of the double-effect ARS with series flow when the effectiveness factors of the solution heat exchangers are optimization variables and are allowed to vary between 0 and 1 – Optimal design (HTA values) and operating conditions (values of temperature, pressure, composition, and mass flow rate) are simultaneously optimized – Significant reductions of TAC, CAPEX, and OPEX values are obtained, compared to the optimized conventional structure of the double-effect ARS with series flow as well as to the optimized conventional configuration of the single-effect ARS	– The overall heat transfer coefficient values to calculate the heat loads in the process units are considered constant – A simplified cost model is employed – Pressure drops are not considered in pipes and heat exchangers – Heat losses are not considered in the process units
Opportunities	**Threats**
– This approach can be applied to optimize ARSs with other series flow – e.g. solution-to-LTG-first −, parallel flow as well as reverse flow – All these flow patterns of the double-effect ARSs can be embedded in a unique representation of the system – a superstructure model – to obtain the optimal pattern for the same target specifications – The same approach can also be applied to optimize, for instance, three-effect ARSs	– A global optimal solution cannot be mathematically guaranteed because the employed optimization solver is based on a local search algorithm. However, numerous model executions starting from different initialization points lead to the same optimal solution. The initial guess values were proposed based on the insights gathered from the optimization of the single-effect ARS as well as on simulation results for the double-effect configuration reported in the literature

evaporator temperature constant at 4 °C. Interestingly, the optimal configuration obtained for the examined ranges of values is the same as the configuration obtained in OptSol 2, i.e. the low-temperature solution heat exchanger LTSHE is (always) eliminated from the conventional double-effect H_2O-LiBr ARS with series flow studied in this work. The contributions of the different process units to the optimal CAPEX depend on the values of the cooling water temperature. For example, if

T_{18} and T_{22} are equal to 15 °C, the EVAP contributes the most to CAPEX for Q_{EVAP} values ranging between 150 and 300 kW; the EVAP and the ABS contribute in the same proportion for Q_{EVAP} of 350 kW; and the ABS is the largest contributor to CAPEX for Q_{EVAP} higher than 350 kW. Finally, if T_{18} and T_{22} are equal to 35 °C, the ABS is the largest contributor to the optimal CAPEX regardless of the Q_{EVAP} value, and its relative contribution increases with increasing Q_{EVAP} values. The

optimization results obtained for the examined ranges of values are provided as Supplementary material to this article.

4.4. Comparison of optimization results between the examined double-effect configurations and the traditional single-effect configuration

As a final analysis, the same optimization problem – minimization of the TAC (Eq. (36) − is solved for the conventional single-effect ARS configuration (Fig. 5) considering the same cost model and parameter values, and design specifications. The obtained optimal solution for the single-effect configuration is named OptSol SE, and is compared to the optimal solutions obtained for the double-effect configurations OptSol 1 and OptSol 2 in Figs. 6 and 7. In this case, the obtained optimal ε_{SHE} value is 0.85.

Compared to OptSol 2 in Fig. 6, the TAC, CAPEX, and OPEX values for OptSol SE increase by 47.7, 42.6, and 62.1%, respectively, while compared to OptSol 1 they increase by 33.6, 26.8, and 54.2%, respectively. According to Fig. 7, the process units that mostly increase in their HTA are the condenser COND (15.8 times and 14.9 times with respect to OptSol 2 and OptSol 1, respectively) and the absorber ABS (51.6% and 33.5% with respect to OptSol 2 and OptSol 1, respectively).

Regarding OPEX, the increase of the cooling utility cost in the single-effect configuration is more significant than the increase of the heating utility cost compared to OptSol 2 and OptSol 1. Indeed, the cooling utility cost increases by 104.8% with respect to OptSol 2, and by 63.9% with respect to OptSol 1, while the heating utility cost increases by 35.3% and 46.0%, respectively.

4.5. Analysis of strengths, weaknesses, opportunities, and threats

A SWOT analysis of the simultaneous optimization approach of the design and operating conditions applied in this paper is presented in Table 10.

5. Conclusions and future work

An optimal configuration for double-effect H_2O-LiBr ARSs with "solution-to-HTG-first" series flow is obtained through a minimization of the TAC. To this end, a mathematical programming approach is employed. Based on the available process unit models and a cost model as well as parameter values, a new process configuration is obtained by solving a nonlinear process model. As a result, the low-temperature solution heat exchanger is eliminated in the optimal solution. This process is obtained if (i) the TAC of the system is minimized, (ii) the trade-offs among all involved process units (sizes: heat transfer areas) and streams (operating conditions: pressure, temperature, solution concentration, and flow rate) are simultaneously elucidated, and (iii) the effectiveness factors of the two solution heat exchangers are allowed to vary between 0 and 1. Published works which mainly focus on energy or exergy analyses, assume effectiveness factor values for the heat exchangers ranging between 0.5 and 0.9, thus always forcing their presence in the process configuration. In this case, by allowing the heat exchanger effectiveness factor to take any value, the trade-offs between investment and operating costs lead to the deletion of the low-temperature solution heat exchanger from the conventional double-effect configuration and to a reduction of the heat transfer area of the absorber (also in the low-temperature zone), but increase the area of the high-temperature solution heat exchanger and the high-temperature generator when the TAC is minimized. That is, the energy integration between the weak and strong LiBr solutions takes place entirely at the high-temperature zone and the other process units, and the operating conditions accommodate accordingly in order to meet the problem specification with the minimal TAC.

The obtained new process configuration allows reducing the TAC, the CAPEX, and the OPEX by around 9.5%, 11.1% and 4.9%,

respectively, with respect to the optimized conventional double-effect configuration with solution-to-HTG-first series flow.

Finally, for the same model inputs, data, and process specifications, the optimal TAC, CAPEX and OPEX obtained for the single-effect configuration are, respectively, 33.6%, 26.8%, and 54.2% higher than the values obtained for the conventional double-effect configuration, and 47.7%, 42.6%, and 62.1% higher than the values obtained for the new double-effect configuration.

In future work, the process unit models will be refined by including the dependence of the overall heat transfer coefficients on temperature. Double-effect configurations with parallel and reverse flow patterns will be individually modeled, optimized, and compared to the solutions presented in this work. Afterwards, a superstructure-based representation of the double-effect process embedding different flow patterns will be modeled and optimized through mathematical programming.

Appendix A. Supplementary material

Supplementary data associated with this article can be found, in the online version, at http://dx.doi.org/10.1016/j.enconman.2017.12.079.

References

[1] Kaynakli O, Kilic M. Theoretical study on the effect of operating conditions on performance of absorption refrigeration system. Energy Convers Manag 2007;48:599–607. http://dx.doi.org/10.1016/j.enconman.2006.06.005.
[2] Sun J, Fu L, Zhang S. A review of working fluids of absorption cycles. Renew Sustain Energy Rev 2012;16:1899–906. http://dx.doi.org/10.1016/j.rser.2012.01.011.
[3] McQuiston FC, Parker JD, Spitler JD. Heating, ventilating and air conditioning analysis and design. 6th ed. Hoboken, NJ: Wiley; 2004.
[4] Mazzei MS, Mussati MC, Mussati SF. NLP model-based optimal design of LiBr–H2O absorption refrigeration systems. Int J Refrig 2014;38:58–70. http://dx.doi.org/10.1016/j.ijrefrig.2013.10.012.
[5] Garousi Farshi L, Mahmoudi SMS, Rosen MA, Yari M, Amidpour M. Exergoeconomic analysis of double effect absorption refrigeration systems. Energy Convers Manag 2013;65:13–25. http://dx.doi.org/10.1016/j.enconman.2012.07.019.
[6] Srikhirin P, Aphornratana S, Chungpaibulpatana S. A review of absorption refrigeration technologies. Renew Sustain Energy Rev 2001;5:343–72. http://dx.doi.org/10.1016/S1364-0321(01)00003-X.
[7] Garousi F, Seyed M, Rosen MA, Yari M. A comparative study of the performance characteristics of double-effect absorption refrigeration systems. Int J Energy Res 2012;36:182–92. http://dx.doi.org/10.1002/er.1791.
[8] Kaushik SC, Arora A. Energy and exergy analysis of single effect and series flow double effect water–lithium bromide absorption refrigeration systems. Int J Refrig 2009;32:1247–58. http://dx.doi.org/10.1016/j.ijrefrig.2009.01.017.
[9] Kaynakli O, Saka K, Kaynakli F. Energy and exergy analysis of a double effect absorption refrigeration system based on different heat sources. Energy Convers Manag 2015;106:21–30. http://dx.doi.org/10.1016/j.enconman.2015.09.010.
[10] Gomri R. Second law comparison of single effect and double effect vapour absorption refrigeration systems. Energy Convers Manag 2009;50:1279–87. http://dx.doi.org/10.1016/j.enconman.2009.01.019.
[11] Talukdar K, Gogoi TK. Exergy analysis of a combined vapor power cycle and boiler flue gas driven double effect water–LiBr absorption refrigeration system. Energy Convers Manag 2016;108:468–77. http://dx.doi.org/10.1016/j.enconman.2015.11.020.
[12] Morosuk T, Tsatsaronis G. A new approach to the exergy analysis of absorption refrigeration machines. Energy 2008;33:890–907. http://dx.doi.org/10.1016/j.energy.2007.09.012.
[13] Morosuk T, Tsatsaronis G. Advanced exergetic evaluation of refrigeration machines using different working fluids. Energy 2009;34:2248–58. http://dx.doi.org/10.1016/j.energy.2009.01.006.
[14] Misra RD, Sahoo PK, Gupta A. Thermoeconomic evaluation and optimization of a double-effect H2O/LiBr vapour-absorption refrigeration system. Int J Refrig 2005;28:331–43. http://dx.doi.org/10.1016/j.ijrefrig.2004.09.006.
[15] Bereche RP, Palomino RG, Nebra SA. Thermoeconomic analysis of a single and double-effect LiBr/H2O absorption refrigeration system. Int J Thermodyn 2009;12:89–96.
[16] Garousi Farshi L, Seyed Mahmoudi SM, Rosen MA. Analysis of crystallization risk in double effect absorption refrigeration systems. Appl Therm Eng 2011;31:1712–7.

http://dx.doi.org/10.1016/j.applthermaleng.2011.02.013.

[17] Arun MB, Maiya MP, Murthy SS. Equilibrium low pressure generator temperatures for double-effect series flow absorption refrigeration systems. Appl Therm Eng 2000;20:227–42. http://dx.doi.org/10.1016/S1359-4311(99)00029-0.

[18] Arun MB, Maiya MP, Murthy SS. Performance comparison of double-effect parallel-flow and series flow water–lithium bromide absorption systems. Appl Therm Eng 2001;21:1273–9. http://dx.doi.org/10.1016/S1359-4311(01)00005-9.

[19] Gebreslassie BH, Medrano M, Boer D. Exergy analysis of multi-effect water–LiBr absorption systems: from half to triple effect. Renew Energy 2010;35:1773–82. http://dx.doi.org/10.1016/j.renene.2010.01.009.

[20] Gebreslassie BH, Groll EA, Garimella SV. Multi-objective optimization of sustainable single-effect water/lithium bromide absorption cycle. Renew Energy 2012;46:100–10. http://dx.doi.org/10.1016/j.renene.2012.03.023.

[21] Morosuk T, Tsatsaronis G. Strengths and limitations of advanced exergetic analyses 2013:V06BT07A026. doi: 10.1115/IMECE2013-64320.

[22] El-Sayed YM, Gaggioli RA. A critical review of second law costing methods—I: background and algebraic procedures. J Energy Resour Technol 1989;111:1–7. http://dx.doi.org/10.1115/1.3231396.

[23] Mussati SF, Aguirre PA, Scenna NJ. Novel configuration for a multistage flash-mixer desalination system. Ind Eng Chem Res 2003;42:4828–39. http://dx.doi.org/10.1021/ie020318v.

[24] Druetta P, Aguirre P, Mussati S. Minimizing the total cost of multi effect evaporation systems for seawater desalination. Desalination 2014;344:431–45. http://dx.doi.org/10.1016/j.desal.2014.04.007.

[25] Oliva DG, Francesconi JA, Mussati MC, Aguirre PA. Modeling, synthesis and optimization of heat exchanger networks. Application to fuel processing systems for PEM fuel cells. Int J Hydrogen Energy 2011;36:9098–114. http://dx.doi.org/10.1016/j.ijhydene.2011.04.097.

[26] Oliva DG, Francesconi JA, Mussati MC, Aguirre PA. Energy efficiency analysis of an integrated glycerin processor for PEM fuel cells: comparison with an ethanol-based system. Int J Hydrogen Energy 2010;35:709–24. http://dx.doi.org/10.1016/j.ijhydene.2009.10.082.

[27] Serralunga FJ, Mussati MC, Aguirre PA. Model adaptation for real-time optimization in energy systems. Ind Eng Chem Res 2013;52:16795–810. http://dx.doi.org/10.1021/ie303621j.

[28] Arias AM, Mussati MC, Mores PL, Scenna NJ, Caballero JA, Mussati SF. Optimization of multi-stage membrane systems for CO2 capture from flue gas. Int J Greenhouse Gas Control 2016;53:371–90. http://dx.doi.org/10.1016/j.ijggc.2016.08.005.

[29] Manassaldi JI, Arias AM, Scenna NJ, Mussati MC, Mussati SF. A discrete and continuous mathematical model for the optimal synthesis and design of dual pressure heat recovery steam generators coupled to two steam turbines. Energy 2016;103:807–23. http://dx.doi.org/10.1016/j.energy.2016.02.129.

[30] Rubio-Maya C, Pacheco-Ibarra JJ, Belman-Flores JM, Galván-González SR, Mendoza-Covarrubias C. NLP model of a LiBr–H2O absorption refrigeration system for the minimization of the annual operating cost. Appl Therm Eng 2012;37:10–8. http://dx.doi.org/10.1016/j.applthermaleng.2011.12.035.

[31] Gebreslassie BH, Guillén-Gosálbez G, Jiménez L, Boer D. Design of environmentally conscious absorption cooling systems via multi-objective optimization and life cycle assessment. Appl Energy 2009;86:1712–22. http://dx.doi.org/10.1016/j.apenergy.2008.11.019.

[32] Mussati SF, Gernaey KV, Morosuk T, Mussati MC. NLP modeling for the optimization of LiBr-H2O absorption refrigeration systems with exergy loss rate, heat transfer area, and cost as single objective functions. Energy Convers Manag 2016;127:526–44. http://dx.doi.org/10.1016/j.enconman.2016.09.021.

[33] Gomri R, Hakimi R. Second law analysis of double effect vapour absorption cooler system. Energy Convers Manag 2008;49:3343–8. http://dx.doi.org/10.1016/j.enconman.2007.09.033.

[34] Dincer I. Refrigeration systems and applications. Wiley; 2003.

[35] Zinet M, Rulliere R, Haberschill P. A numerical model for the dynamic simulation of a recirculation single-effect absorption chiller. Energy Convers Manag 2012;62:51–63. http://dx.doi.org/10.1016/j.enconman.2012.04.007.

[36] American Society of Heating R and A-CE. 1989 ASHRAE handbook: fundamentals. Atlanta, GA: ASHRAE; 1989.

[37] Boryta DA, Maas AJ, Grant CB. Vapor pressure-temperature-concentration relation for system lithium bromide and water (40–70% lithium bromide). J Chem Eng Data 1975;20:316–9. http://dx.doi.org/10.1021/je60066a017.

[38] Rogers G, Mayhew Y. Engineering thermodynamics: work and heat transfer. 4th ed. Harlow, Essex, England; New York: Longman Scientific; 1992.

[39] Matches' 275 Equipment Cost Estimates. n.d. < http://www.matche.com/equipcost/Default.html > (accessed June 22, 2017).

[40] GAMS Development Corporation. General Algebraic Modeling System (GAMS) Release 23.6.5. Washington, DC, USA: 2010.

[41] Drud A. CONOPT 3 solver manual. Bagsvaerd, Denmark: ARKI Consulting and Development A/S; 2012.